

The climate subsystem in IMAGE updated to MAGICC 6.0

Background Studies

The climate subsystem in IMAGE updated to MAGICC 6.0

M. Schaeffer, E. Stehfest



Netherlands Environmental Assessment Agency

The climate subsystem in IMAGE updated to MAGICC 6.0

© Netherlands Environmental Assessment Agency (PBL), June 2010

PBL publication number 500110005

Corresponding Author: Elke.Stehfest@pbl.nl; IMAGE-info@pbl.nl

Parts of this publication may be reproduced, providing the source is stated, in the form:
Netherlands Environmental Assessment Agency: The climate subsystem in IMAGE updated to
MAGICC 6.0.

This publication can be downloaded from our website: www.pbl.nl/en. A hard copy may be
ordered from: reports@pbl.nl, citing the PBL publication number.

The Netherlands Environmental Assessment Agency (PBL) is the national institute for
strategic policy analysis in the field of environment, nature and spatial planning. We contribute
to improving the quality of political and administrative decision-making by conducting outlook
studies, analyses and evaluations in which an integrated approach is considered paramount.
Policy relevance is the prime concern in all our studies. We conduct solicited and unsolicited
research that is both independent and always scientifically sound.

Office Bilthoven
PO Box 303
3720 AH Bilthoven
The Netherlands
Telephone: +31 (0) 30 274 274 5
Fax: +31 (0) 30 274 44 79

Office The Hague
PO Box 30314
2500 GH The Hague
The Netherlands
Telephone: +31 (0) 70 328 8700
Fax: +31 (0) 70 328 8799

Rapport in het kort

Het simpele klimaatmodel MAGICC vormt de kern van het klimaatsysteem AOS (Atmosfeer-Oceaan Systeem) in het model IMAGE (“Integrated Model to Assess the Global Environment”) van het PBL. MAGICC is gebuikt in de derde en vierde assessment rapporten van het IPCC (International Panel for Climate Change), als centraal model om de gevolgen door te rekenen van een groot aantal scenario’s van broeikasgasconcentraties voor het mondiaal gemiddelde klimaat. Sinds de publicatie van die rapporten is het MAGICC model grondig herzien om beter de resultaten van geavanceerde gekoppelde klimaatmodellen (Atmosphere-Ocean General Circulation Models, AOGCMs) te kunnen nabootsen. De reeks van verbeteringen aan MAGICC zijn geïmplementeerd in IMAGE-AOS, om IMAGE 2.5 up-to-date te maken met de nieuwste ontwikkelingen in de klimaatmodellering. Dit rapport presenteert de details van deze update en de nieuwe kalibratie van het model, evenals de overeenkomsten en verschillen met de vorige IMAGE versie en met het nieuwe MAGICC 6.0 model.

Het grootste voordeel van het nieuwe IMAGE model is dat het met MAGICC 6.0 via het instellen van een aantal (nieuwe) parameters de tijdsafhankelijke response van AOGCMs kan reproduceren voor uiteenlopende scenario’s, zodat interacties in het klimaatsysteem en de gevolgen van toekomstige klimaatverandering beter kunnen worden afgebeeld.

Trefwoorden / Keywords:

IMAGE; AOS; MAGICC; klimaatmodel/ climate model; kalibratie/calibration.

Inhoud

- Rapport in het kort 5
- Summary 9
- 1 Introduction 11
- 2 Amendments in IMAGE-AOS 13
 - 2.1 The Atmosphere-Ocean System: A bird's eye view 13
 - 2.2 The Energy-Balance / Upwelling-Diffusion model 14
 - 2.3 Update of radiative forcing agents 19
- 3 Testing the IMAGE-AOS update 21
 - 3.1 Comparing to MAGICC 6.0 and testing new parameters 21
 - 3.2 CO₂ concentration 22
 - 3.3 Comparison with IMAGE 2.3 23
 - 3.4 Scenario projections for various AOGCM emulations 23
- 4 Conclusions 29
- References 30
- Colophon 31

Summary

The simple climate model MAGICC is part of the Atmosphere-Ocean System (AOS) within the IMAGE model (“Integrated Model to Assess the Global Environment”) of PBL. The MAGICC model was used extensively in the Third and Fourth Assessment Reports of IPCC (Intergovernmental Panel on Climate Change) for running a range of greenhouse gas concentration scenarios. Since the publication of these reports, the MAGICC model has been updated to improve its emulation of results from Atmosphere-Ocean General Circulation Models (AOGCMs). The series of improvements to the MAGICC model have been implemented in IMAGE-AOS, to bring IMAGE 2.5 up-to-date with the most recent developments in climate modelling. This report presents details about the improvements and the re-calibration of the model, it shows the model results and discusses the similarities and differences with the previous IMAGE versions and the new MAGICC 6.0 version.

The single most important advantage of the new IMAGE model is that, in combination with MAGICC 6.0, the model can reproduce the time-dependent response of AOGCMs for various scenarios, by adjusting the values of a limited number of parameters. This makes the IMAGE model better suited to provide plausible projections of future climate-change feedbacks and impacts.

Introduction

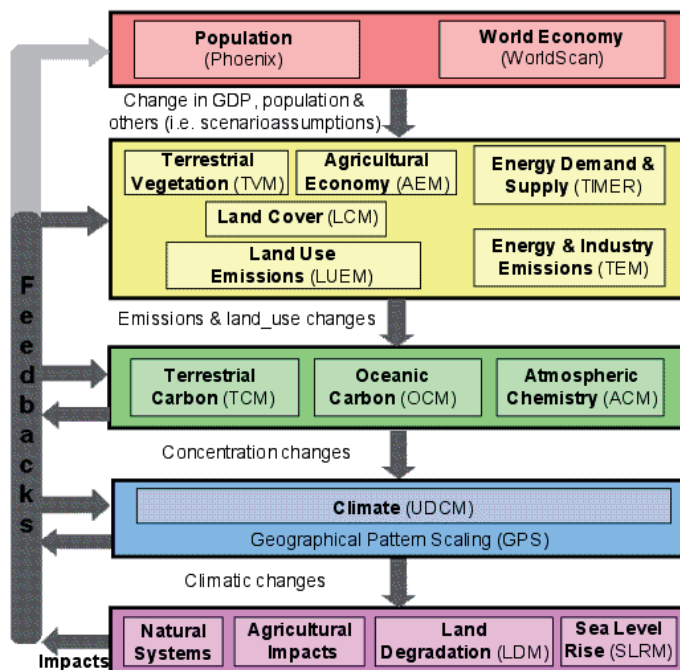


IMAGE (Integrated Model to Assess the Global Environment) is the in-house model of the Netherlands Environmental Assessment Agency (PBL) for exploring the coarse resolution, and mid- to long-term dynamics of global environmental change. Based on scenarios of future socio-economic developments, the model simulates changes in energy supply and demand, land-use change, changes in natural vegetation patterns, the carbon cycle of land and ocean, the chemical composition of the atmosphere and changes in climate, including temperature and precipitation. Crucially, the IMAGE model represents many feedbacks between the subsystems, such as the impact of climatic change on vegetation patterns, crop yields and the carbon cycle (see Figure 1). An important link in the chain of impacts and feedbacks is the Atmosphere-Ocean System (AOS).

In 2004, the IMAGE model was provided with a major update of AOS (Eickhout *et al.*, 2004). For example, the two-dimensional climate model in IMAGE 2.1 (De Haan *et al.*, 1994) was replaced by the climate core of the well-supported and validated model MAGICC (Hulme *et al.*, 2000). Climate change in MAGICC is calculated by a upwelling-diffusion climate model (UDCM). MAGICC has been used as the central simple climate model (SCM) in the third assessment report of the IPCC (Intergovernmental Panel on Climate Change) and in the IPCC's fourth assessment report (Meehl *et al.*, 2007). This UDCM version was used in IMAGE 2.2, 2.3 and 2.4.

However, since the publication of the third and fourth assessment reports of the IPCC, the MAGICC model has been thoroughly updated (Meinshausen *et al.*, 2008), to

Figure 1.1



Schematic overview of IMAGE (IMAGE team 2001). The Atmosphere-Ocean System consists of the Oceanic Carbon model, the Atmospheric Chemistry model, the (Upwelling-Diffusion) Climate model and the Sea Level Rise model*. * The Terrestrial Carbon Model (TCM) of IMAGE 2.2 forms part of the Terrestrial Environment System (TES). This distinction is made because of the grid detail of TCM (0.5 by 0.5 degrees) compared to the global-mean scale of the Ocean Carbon Model (OCM).

improve its ability to emulate the time-evolution of mean global climate, as simulated by a range of AOGCMs (coupled Atmosphere-Ocean General Circulation Models). The new MAGICC 6.0 version contains several new parameterisations and calibrated parameters. Not all of these are relevant to the IMAGE model. In particular, the IMAGE model contains a different, more detailed description of the terrestrial carbon cycle, highly suited to the type of scenario analysis at the PBL. Thus, the carbon cycle in the MAGICC model is not adopted for the IMAGE model.

The next chapter describes those parts of the MAGICC model that have changed and were adopted in the IMAGE model. Together with other changes to the model, the version number was increased to IMAGE 2.5 (when moving from version 2.2 to 2.3 and 2.4, AOS had not been changed). Chapter 3 presents results from the previous and updated versions of IMAGE-AOS, and MAGICC 6.0, for both the historical period and several scenario projections.

In this report, we present the changes in AOS by drawing from the 2004 AOS report (Eickhout *et al.*, 2004). Parts of the 2004 AOS report were copied and adapted to make reporting of the amendments here more efficient. A full description of the AOS modules that were not updated can be obtained from Eickhout *et al.* (2004).

Schematic overview of IMAGE (IMAGE team 2001). The Atmosphere-Ocean System consists of the Oceanic Carbon model, the Atmospheric Chemistry model, the (Upwelling-Diffusion) Climate model and the Sea Level Rise model¹

¹ The Terrestrial Carbon Model (TCM) of IMAGE 2.2 forms part of the Terrestrial Environment System (TES). This distinction is made because of the grid detail of TCM (0.5 by 0.5 degrees) compared to the global-mean scale of the Ocean Carbon Model (OCM).

Amendments in IMAGE-AOS

Because of differences in development history, objectives and applications, IMAGE cannot adopt all improvements to the MAGICC model that are described in Meinshausen *et al.* (2008). The changes in the upwelling-diffusion climate model have been fully adopted, but those in the calculation of radiative forcing have only partly been adopted and the changes in the carbon cycle not at all. Following a short overview of AOS, the updates and amendments are presented in detail.

2.1 The Atmosphere-Ocean System: A bird's eye view

The main goal of AOS is to compute transient climate changes that result from changes in greenhouse gas emissions, in a way that is computationally more economic than a three-dimensional atmospheric chemistry model coupled with an AOGCM. This allows for a dynamic link between AOS and the Terrestrial Environmental System (TES), and for using the entire IMAGE model iteratively for policy analysis. This approach also makes it possible to investigate different feedbacks and linkages between the society-biosphere-climate system, which would be impossible with a complex three-dimensional coupling of atmospheric and ocean models. The faster computations are obtained at the expense of a lower degree of complexity and detail, compared to GCMs and three-dimensional atmospheric chemistry models.

AOS consists of the Atmospheric Chemistry Model, the Oceanic Carbon Model, the Upwelling-Diffusion Climate Model, the Sea-Level Rise Model, and the Geographical Pattern Scaling model (GPS). The first four models are zero-dimensional or one-dimensional, mean global models. The most important variables (global temperature and precipitation change) are scaled to the TES grid level (0.5 by 0.5 degrees in the horizontal) by the Geographical Pattern Scaling model (GPS) to allow linkage with TES. Figure 2.1 shows the linkages between the AOS sub-models, in terms of input and output variables.

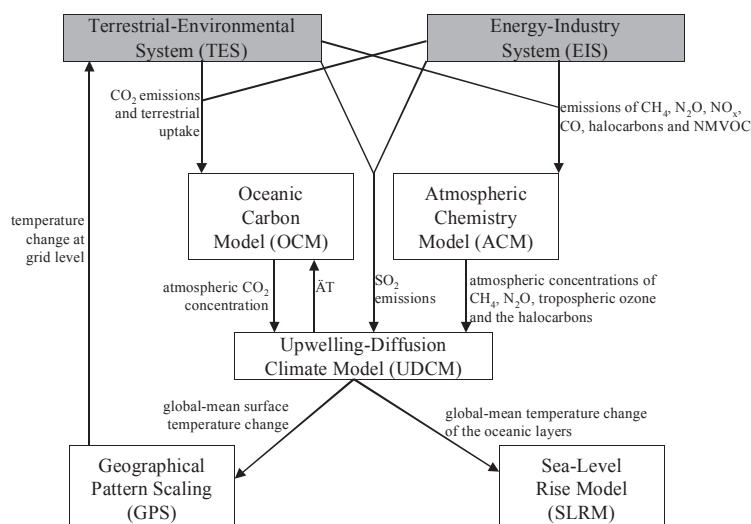
Below, a short description is given of the five AOS models as used in IMAGE 2.2, 2.3, 2.4 and 2.5:

- The Atmospheric Chemistry Model (ACM). The ACM model, an updated version of the IMAGE 2.1 globally averaged chemistry module (Krol and Van der Woerd, 1994), calculates the atmospheric build-up of greenhouse gases and other atmospheric substances relevant to global

change. The emissions of methane (CH₄), nitrogenous oxide (N₂O), carbon monoxide (CO), non-methane volatile organic compounds (NMVOC), nitrogen oxide (NO_x) and halocarbons (CFCs, HCFCs, HFCs, Halon-1211, Halon-1301 and CH₃Br), are used as input. The atmospheric concentrations of CH₄, N₂O, CO, the OH radical, and tropospheric ozone (O₃), are calculated by the ACM model. It was not updated in IMAGE 2.5, and is identical to what is included in IMAGE versions 2.2, 2.3 and 2.4; a full description can be obtained from Eickhout *et al.* (2004).

- The Oceanic Carbon Model (OCM). The OCM model, which calculates the carbon uptake by the oceans, consists of a mean global response function that responds to changes in anthropogenic and terrestrial CO₂ fluxes and changes in the temperature of the oceanic mixed layer. The output of the OCM model is the net flux of CO₂ and, consequently, its atmospheric concentration. The model is based on the Bern Oceanic Carbon Cycle model (Joos *et al.*, 1996), and was not updated in IMAGE 2.5; a full description can be obtained from Eickhout *et al.* (2004). An update was not necessary, as MAGICC 6.0 now includes the same Bern Oceanic Carbon Cycle model (Joos *et al.*, 1996) as is included in the IMAGE model.
- The Upwelling-Diffusion Climate Model (UDCM). The UDCM model first converts the of greenhouse gas concentrations (from OCM and ACM) and SO₂ emissions (from TES and EIS) into radiative forcings. Subsequently, these radiative forcings are used as input to calculate the mean global surface and ocean temperature change. For IMAGE 2.5, this part of AOS was updated, based on Meinshausen *et al.* (2008), as described in the remainder of this report.
- The Geographical Pattern Scaling Model (GPS). The GPS model scales the mean global surface temperature change to a grid level of 0.5 by 0.5 degrees. This scaling is applied to changes in temperature and precipitation. GCM results based on experiments with forcings from sulphate only are also used for taking the non-linear regional effects of sulphate aerosols into account. Results from the AGC/MLO model (11-layer troposphere/lower-stratosphere general circulation/mixed-layer-ocean) from the University of Illinois at Urbana-Champaign (UIUC) are used for these sulphate-only patterns¹. The complete method is described by Schlesinger *et al.* (2000). The method is not updated in

¹ The sulphur patterns were kindly provided by Michael Schlesinger and Sergej Malyshev.



Flow diagram of the Atmosphere-Ocean System (AOS) in IMAGE 2.2, 2.3, 2.4 and 2.5. The land-use and natural emissions (including terrestrial uptake of CO₂) from TES and energy and industry emissions from EIS represent the AOS input. Concentration changes, changes in radiative forcing, temperature changes and sea level rise are outputs of AOS. The mean global temperature change of the oceanic mixed layer is used as input for the oceanic carbon model.

IMAGE 2.5; a full description can be obtained from Eickhout *et al.* (2004).

- The Sea-Level Rise Model (SLRM). The SLRM model is based on the model on sea level rise in the MAGICC climate model (Raper *et al.*, 1996), and calculates the mean global sea level rise. The new MAGICC version contains no updates for sea level rise, a full description can be obtained from Eickhout *et al.*, (2004).

2.2 The Energy-Balance / Upwelling-Diffusion model

2.2.1 The energy-balance model

This model consists of an atmosphere box, coupled to northern hemisphere (NH) and southern hemisphere (SH) land and ocean boxes (see Figure 2.2). In IMAGE 2.2, 2.3 and 2.4, the two ocean boxes are each divided into 40 layers, with a mixed layer on top that absorbs the energy of solar radiation. In IMAGE 2.5, the number of layers has been increased to 50. Above land, no energy is assumed to be absorbed.

The energy balance of the climate system can be described as:

$$\Delta Q = \lambda \Delta T_a + \Delta F \quad (1)$$

where ΔQ is the global increase in radiative forcing ($W \cdot m^{-2}$) and ΔF the net heat flux into the ocean ($W \cdot m^{-2}$). Both fluxes are averaged over the entire world area. The term $\lambda \Delta T_a$ is the change in the rate of heat loss to outer space from the climate system. The feedback parameter λ ($W \cdot m^{-2} \cdot C^{-1}$) is inversely related to the climate sensitivity (ΔT_{2x}): the long-term (equilibrium) annual and mean global surface air

temperature increase for a doubling of CO₂ concentration from its pre-industrial level (Houghton *et al.*, 1996). The climate sensitivity is a very important factor for determining the response of the climate system (in terms of temperature change) to changes in CO₂. In equilibrium, the net heat flux into the ocean is zero, so that for a doubling of the CO₂ concentration:

$$\Delta Q_{2x} = \lambda_{2x} \Delta T_{2x} \Rightarrow \lambda_{2x} = \frac{\Delta Q_{2x}}{\Delta T_{2x}} \quad (2)$$

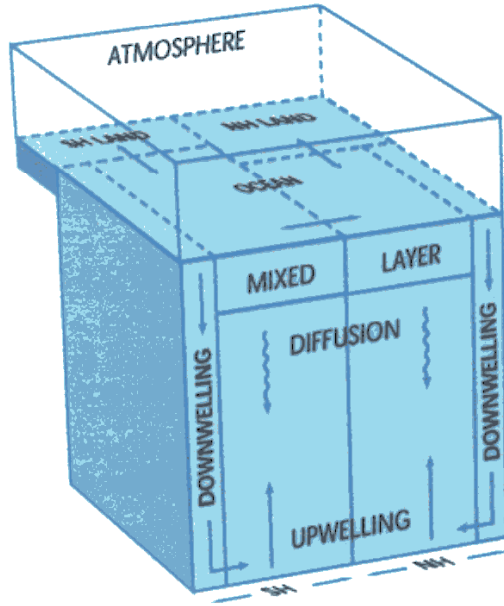
In IMAGE 2.5, the feedback parameter is now a function of the forcing, to reflect that, as found in some GCMs, the climate system responds more strongly to high forcing:

$$\lambda = \frac{\Delta Q_{2x}}{\lambda_{2x} + \xi(\Delta Q - \Delta Q_{2x})} \quad (3)$$

For a value of zero for the parameter ξ , the feedback parameter is equal to λ_{2x} and IMAGE 2.5 behaves like the versions 2.2, 2.3 and 2.4. For any other value of ξ , the feedback parameter λ is also equal to λ_{2x} if the forcing ΔQ is equal to ΔQ_{2x} . If $\xi > 0$, then forcings higher than ΔQ_{2x} will reduce λ to a value smaller than λ_{2x} , thus the ‘transient’, or ‘effective’ climate sensitivity will be higher than ΔT_{2x} (via the inverse relation (2))

Equation (1) partitions the radiative forcing between increased heat loss to outer space and additional uptake of heat by the climate system (Raper *et al.*, 2001). On time scales relevant to anthropogenic climate change, the changes in the atmosphere can be assumed to be in equilibrium with the underlying oceanic mixed layer:

$$C_m \frac{d\Delta T_{O,1}}{dt} = \Delta Q - \lambda \Delta T_a - \Delta F \quad (4)$$



The geographical boxes distinguished in the Upwelling-Diffusion Climate Model (Harvey *et al.*, 1997).

where $d\Delta T_{o,1}$ is the temperature change of the oceanic mixed layer, and C_m the effective bulk heat capacity of the oceanic mixed layer (Wigley and Schlesinger, 1985).

2.2.2 Transient energy balance

The distribution of total absorbed heat over the four geographical boxes (Figure 2.2) is determined by k_{LO} and k_{NS} (the land-ocean and northern-southern hemisphere heat-exchange coefficients) and different feedback parameters λ_o and λ_l , for ocean and land. These feedback parameters are calculated from the equilibrium land-ocean warming ratio RLO and other parameters in an updated iterative numerical procedure (Meinshausen *et al.*, 2008).

By specifying the distribution of energy over the individual boxes, Equation 1 can be re-written for the northern hemisphere ocean (NO) as:

$$f_{NO} \left(\rho \cdot c \cdot h_m \frac{d\Delta T_{NO,1}}{dt} - \Delta Q_{NO} + \lambda_o \alpha \Delta T_{NO,1} + \Delta F_{NO} \right) = k_{LO} (\Delta T_{NL} - \alpha \mu \Delta T_{NO,1}) + k_{NS} (\Delta T_{SO,1} - \Delta T_{NO,1}) \quad (5)$$

where f_{NO} is the fraction of ocean area in the northern hemisphere and $C_m = \rho \cdot c \cdot h_m$ the heat capacity of the ocean mixed layer; the product of the density of seawater (ρ), the specific heat capacity of water (c) and the height of the oceanic mixed layer (h_m). $\Delta T_{NO,1}$, $\Delta T_{SO,1}$ and ΔT_{NL} represent the temperature change of the NH ocean mixed layer, SH ocean mixed layer and NH land surface, respectively (all in °C).

The right-hand side of Equation 5 gives the heat-exchange terms between land and ocean in the NH and between the ocean boxes in the NH and SH. The new parameter μ is an amplification factor for an increased effect of changes in ocean temperatures at the land-ocean heat exchange ΔF_{LO} :

$$\Delta F_{LO} = k_{LO} (\Delta T_{NL} - \mu \Delta T_{NO}) \quad (6)$$

where the temperature of air over the ocean, in which α determines the ratio of change in air temperature over the oceans to mixed-layer ocean temperature ($\Delta T_{NO} = \alpha \Delta T_{NO,1}$).

For the NH land surface, assuming zero heat capacity for land, Equation 1 becomes:

$$f_{NL} (-\Delta Q_{NL} + \lambda_l \Delta T_{NL}) = k_{LO} (\alpha \mu \Delta T_{NO,1} - \Delta T_{NL}) \quad (7)$$

Substituting Equation 7 in 5 results in:

$$f_{NO} \left(\rho \cdot c \cdot h_m \frac{d\Delta T_{NO,1}}{dt} - \Delta Q_{NO} + \lambda_o \alpha \Delta T_{NO,1} + \Delta F_{NO} \right) = f_{NL} (\Delta Q_{NL} - \lambda_l \Delta T_{NL}) + k_{NS} (\Delta T_{SO,1} - \Delta T_{NO,1}) \quad (8)$$

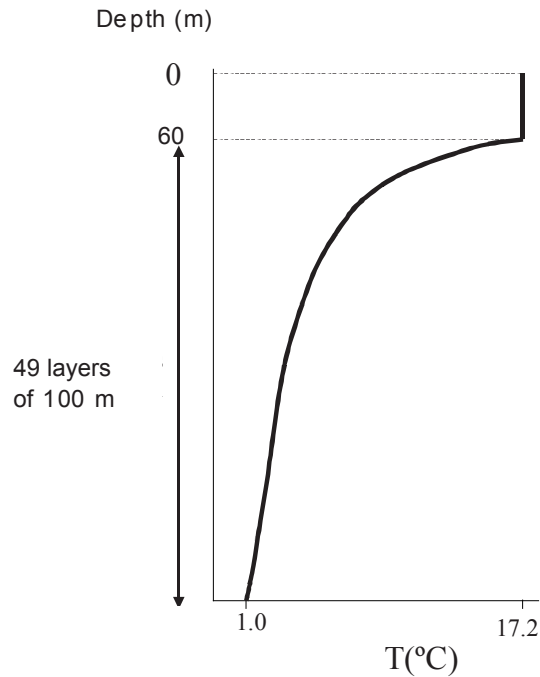
From Equation 8, the time evolution of $\Delta T_{NO,1}$ can be calculated, after ΔF_{NO} is derived from the heat fluxes in the ocean below the mixed layer. The equations for the southern hemisphere are analogous to Equations 5 to 8 for the northern hemisphere.

2.2.3 Upwelling-Diffusion

The ocean is considered one-dimensional, with 50 vertical layers in each hemisphere (40 in IMAGE 2.2, 2.3 and 2.4). The temperature of the mixed layer ($T_{NO,1}$) does not vary with depth, the initial value is 17.2 °C. The bottom layer of the ocean ($T_{NO,50}$) has an initial value of 1.0 °C. The temperature profile between the bottom of the mixed layer and the ocean floor is described by the following equation:

$$T_{NO,n} = T_{NO,nol} + (T_{NO,1} - T_{NO,nol}) \cdot \exp\left(-\frac{w_0 \cdot z(n)}{K_{z,0}}\right) \quad (9)$$

where nol is the number of ocean layers, $n = F, 2, \dots, nol$ (all ocean layers under the mixed layer), w_0 the initial upwelling



The initial temperature profile of the ocean. The temperature in the oceanic mixed layer is considered to be constant with depth.

rate (4.0 m/yr), $z(n)$ is the distance from the bottom of the mixed layer to the middle of each layer (m), and $K_{z,0}$ is the initial value of the vertical diffusivity (m^2/yr).

The initial temperature profile is depicted in Figure 2.3. The height of the mixed layer (h_m) is 60 metres (90m in IMAGE 2.2, 2.3 and 2.4), and the height of the other layers (d) is 100 metres each.

The temperature change in the ocean is derived from:

$$\frac{\partial \Delta T_{NO,n}}{\partial t} = K_z \frac{\partial^2 \Delta T_{NO,n}}{\partial z^2} + w \frac{\partial \Delta T_{NO,n}}{\partial z} \quad (10)$$

where K_z is the vertical diffusivity (m^2/yr), w the upwelling rate (m/yr), z the depth at which the process occurs (m), and t the time step (yrs).

The vertical mixing processes in the ocean are represented by vertical diffusivity and upwelling. In previous versions, the vertical diffusivity was assumed constant with depth and over time. In IMAGE 2.5, the vertical diffusivity changes over time and with depth, to reflect the decrease in vertical mixing with increased stratification of ocean layers; the ocean column becomes more stable as the upper ocean warms, relative to lower layers. The time-dependent vertical diffusivity in layer n is given by:

$$K_{z,n} = \max(K_{z,\min}, (1 - d_n) \frac{\partial K_{z,\text{top}}}{\partial T} (\Delta T_{HO,1} - \Delta T_{HO,nol}) + K_{z,0}) \quad (11)$$

where $K_{z,\min}$ is the minimal vertical diffusivity ($0.1 \text{ m}^2/\text{yr}$), $K_{z,0}$ the initial vertical diffusivity (m^2/yr) and d_n (-) the relative depth of the layer boundary (zero at the bottom of the mixed layer and one at the top of the bottom layer).

$\frac{\partial K_{z,\text{top}}}{\partial T}$ is the parameter determining the sensitivity of the

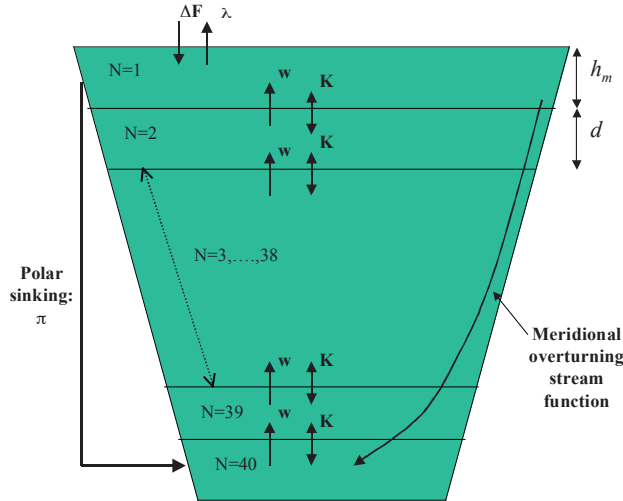
vertical diffusivity to the difference in temperature change between the ocean mixed layer ($\Delta T_{HO,1}$) and the bottom layer ($\Delta T_{HO,nol}$) (where H denotes the respective hemisphere). For

negative values of $\frac{\partial K_{z,\text{top}}}{\partial T}$, the vertical diffusivity decreases

as the contrast in temperature change between the top and bottom layers increases.

The diffusivity and upwelling processes occur between each ocean layer. To implement the thermohaline circulation in this one-dimensional model, a downwelling process is added from the mixed layer to the bottom layer in the polar regions. This process is regulated by the factor π ; the temperature change ratio from polar to non-polar regions. Different GCM simulations show a reduction in the rate of upwelling as greenhouse-gas-induced warming increases (Meehl *et al.*, 2007). This mechanism is handled by applying a relationship between w and the ocean surface temperature change, given by:

$$w(t) = w_0 \left(1 - \frac{\Delta T}{\Delta T^+} \right) \quad (12)$$



Schematic view of the ocean and its main fluxes.

where ΔT^* is a tuneable parameter representing the magnitude of warming that would result in zero upwelling (Raper *et al.*, 1996) and w_0 the initial upwelling rate.

A collapse of the thermohaline circulation would result in a deeper penetration of warm water in the deep ocean. However, a zero upwelling is not likely to occur, not even when the thermohaline circulation has stopped, because of meridional overturning stream functions of the ocean (see Figure 2.4). These functions show a number of isolines in the ocean, returning a flow from high ocean layers in the high latitude regions to oceanic bottom layers in the mid-latitude regions. These flows will partly preserve the existing upwelling in the ocean (Raper *et al.*, 2001). Therefore, Equation 12 is only applied to a fraction of the upwelling, the other fraction is assumed to be constant. In the new model version, the constant fraction of upwelling is 30% (70% in IMAGE 2.2, 2.3 and 2.4), which, combined with an initial upwelling rate $w_0 = F$ 4.0 m/yr and a threshold temperature of $\Delta T^* = F$ 8 °C, results in a medium response of the thermohaline circulation, compared to a range of GCM simulations (Meehl *et al.*, 2007).

Consequently, the function of ΔF_{NO} can be formulated as:

$$\Delta F_{NO} = \frac{\rho \cdot c \cdot K_z (\Delta T_{NO,1} - \Delta T_{NO,2})}{0.5h_d} - \rho \cdot c \cdot w (\Delta T_{NO,2} - \pi \cdot \Delta T_{NO,1}) - \rho \cdot c \cdot \Delta w (\Delta T_{NO,2}^0 - \Delta T_{NO,sink}^0) \quad (13)$$

where $h_d = F$ 100 m (height of the ocean layers below the mixed layer), is the temperature change of the first layer beneath the mixed layer, the initial temperature of this layer, the initial temperature of the downwelling water, and the change in the rate of upwelling with respect to the initial value. The factor 0.5 relates to the application of the diffusion and upwelling process to the middle of each layer.

Equation 13 can be implemented in Equation 8. Moreover, rewriting Equation 7 gives the following calculation of the change in land temperature in the northern hemisphere:

$$\Delta T_{NL} = \frac{f_{NL} \Delta Q_{NL}}{f_{NL} \cdot \lambda_L + k_{LO}} + \frac{k_{LO} \Delta T_{NO,1}}{f_{NL} \cdot \lambda_L + k_{LO}} \quad (14)$$

Implementing Equation 14 in Equation 8 provides a complex calculating scheme for solving the equation for temperature change of the oceanic mixed layer (see Meinshausen *et al.*, 2008).

When the temperature changes of all the oceanic layers are calculated, the temperature change above the land () can be calculated, as well (Equation 14). The mean global temperature change of the total surface layer is derived by the area-weighted mean of the temperature changes in the four geographical boxes.

In IMAGE 2.5, the horizontal area of ocean layers is a function of depth and in each hemisphere equal to that in the Hadley Centre OGCM model. This introduces additional terms in the equations above as detailed in Meinshausen *et al.* (2008).

For further information on the MAGICC model, see Wigley and Raper (1987, 1992, 1993, 1995), Raper *et al.* (1996), Hulme *et al.* (2000) and Meinshausen *et al.* (2008).

	SO ₂	NO _x	BC	OC	Total
Fossil Fuel Emissions Direct Forcing (Wm ²) in 2005	-0.40	-0.10	+0.20	-0.05	-0.35
Biomass Burning Emissions Direct Forcing (Wm ²) in 2005	-0.10	-0.10	+0.38	-0.15	+0.03

2.2.4 Radiative Forcing

Increased concentrations of greenhouse gases in the atmosphere lead to a change in radiative forcing, a measure of the extra energy input in the surface-troposphere system. This radiative forcing leads to an increase in the mean global surface temperature. The input and output of this AOS component is given in the text box below.

Model input	- Atmospheric concentrations of the most important greenhouse gases (CO ₂ , CH ₄ , N ₂ O, tropospheric O ₃ , CFCs, HCFCs, PFCs, Halon-1211, Halon-1301, CH ₃ Br, SF ₆ , CH ₃ CCl ₃ and CH ₃ Cl. - Energy, industry and land-use emissions of aerosol precursors SO ₂ , NO _x , Black Carbon (BC) and Organic Carbon (OC).
Model output	- Changes in radiative forcing for CO ₂ , CH ₄ , N ₂ O, tropospheric O ₃ , stratospheric O ₃ , CFCs, HCFCs, PFCs, Halon-1211, Halon-1301, CH ₃ Br, SF ₆ , CH ₃ CCl ₃ , CH ₃ Cl, stratospheric water vapour and a number of tropospheric aerosols (used as input for the UDCM model).

The parameterisations below are new or have been updated in the IMAGE 2.5 version.

Radiative forcing CO₂

The radiative forcing of carbon dioxide is calculated as:

$$\Delta Q_{CO_2,t} = \alpha_{CO_2} \cdot \ln\left(\frac{[CO_2]_t}{[CO_2]_{t_0}}\right) \quad (15)$$

where t_0 is 1765, the year of initialisation in IMAGE 2 (see Section 3.1). The pre-industrial concentration of CO₂ is assumed to be 278 ppmv. The scaling parameter α_{CO_2} has a default value of 5.325 Wm², leading to an increased forcing of 3.7 Wm² for a doubling of the CO₂ concentration (IPCC, 2001). In the new IMAGE version, this value can be adjusted to emulate GCM results.

Direct radiative forcing effect tropospheric aerosols

In IMAGE 2.2, 2.3 and 2.4, the direct effect of scattering and absorption by tropospheric aerosols was included for sulphate, black carbon and organic carbon, from both fossil-fuel and biomass combustion. For each species s , the direct radiative forcing in a reference year t_{ref} is scaled, using the emissions at time t and in the reference year:

$$\Delta Q_{s,t}^{direct} = \Delta Q_{s,t_{ref}}^{direct} \cdot emis_{s,t} / emis_{s,t_{ref}} \quad (16)$$

In IMAGE 2.5, nitrate aerosol is included, as well, and the reference radiative forcing for each species is updated to the year 2005, following Forster (2007), see the Table 2.1.

Indirect radiative forcing effect tropospheric aerosols

Aerosols serve both as cloud condensation and ice nuclei. As a result, the aerosols change the microphysics, the radiative properties and the lifetime of clouds, and hence, change the cloud albedo and cloud cover. This effect is called the indirect radiative forcing caused by aerosols. Moreover, there are two indirect effects to distinguish: 1) an increase in aerosols, causing an increase in droplet concentration, and 2) the reduction in cloud droplet size, affecting the precipitation efficiency and tending to increase the liquid water content, the cloud lifetime and the cloud thickness (IPCC, 2001). In IMAGE, these two effects are lumped together in a total indirect forcing.

In IMAGE 2.5, the indirect forcing of aerosols is calculated for a mix of sulphate, nitrate, black carbon and organic carbon aerosols, and not just for sulphate alone, as in the previous model versions. Number concentrations of aerosols are approximated by optical thickness in a reference year and scaled with emissions for other years. For each species s the number concentration in year t is:

$$N_{s,t}^{ff} = N_{s,t_{ref}}^{ff} \cdot emis_{s,t}^{ff} / emis_{s,t_{ref}}^{ff} \quad (\text{for fossil fuel emissions}) \quad (17a)$$

$$N_{s,t}^{bb} = N_{s,t_{ref}}^{bb} \cdot emis_{s,t}^{bb} / emis_{s,t_{ref}}^{bb} \quad (\text{for biomass burning emissions}) \quad (17b)$$

$$N_{s,t}^n = N_{s,t_{ref}}^n \cdot emis_{s,t}^n / emis_{s,t_{ref}}^n \quad (\text{for natural emissions}) \quad (17c)$$

Total number concentrations from all sources are normalised in the reference year for each species:

$$N_{s,t} = \left(N_{s,t}^{ff} + N_{s,t}^{bb} + N_{s,t}^n \right) \left(N_{s,t_{ref}}^{ff} + N_{s,t_{ref}}^{bb} + N_{s,t_{ref}}^n \right) \quad (18)$$

When the various sources for each species are grouped together, using Equation (17), an additional factor 0.75 is introduced for Black Carbon from fossil-fuel combustion, to account for the differential solubility from industrial (fossil-fuel) and biomass combustion.

Finally, in the calculation of total indirect forcing, all different species are grouped together weighted by a factor w_s , according to an estimate of their relative impact as cloud nuclei. These factors are estimated as 36%, 23%, 36% and 5%, for SO_x, NO_x, BC and OC, respectively, but are highly uncertain (Hansen *et al.*, 2005).

The impact of changes in aerosol number concentrations on total indirect forcing follows a logarithmic relationship, relating the concentrations at time t to those under pre-industrial conditions.

$$\log^{10} \left(\frac{\sum_s w_s \cdot N_{s,t}}{\sum_s w_s \cdot N_{s,pf}} \right)$$

This functional relation is normalised in a reference year to scale the estimated indirect forcing in the reference year ($\Delta Q_{ref}^{indirect}$), for which: $\sum_s w_s \cdot N_{s,t} = 1$

$$\Delta Q_t^{indirect} = \Delta Q_{ref}^{indirect} \cdot \log^{10} \left(\frac{\sum_s w_s \cdot N_{s,t}}{\sum_s w_s \cdot N_{s,PI}} \right) \bigg/ \log^{10} \left(\frac{1}{\sum_s w_s \cdot N_{s,PI}} \right) \quad (19)$$

For the year 2005, the reference total indirect forcing $\Delta Q_{ref}^{indirect}$ is -0.7 Wm^2 .

Efficacy and forcing patterns for forcing agents

Radiative forcing is a measure of the energy imbalance of the Earth's troposphere system. In the field of climate change, a change in radiative forcing is caused by changes in atmospheric composition, reflection by (or near) the Earth's surface, or radiative input at the top of the atmosphere. Radiative forcing is a central concept in the energy-balance modelling in IMAGE. However, to a certain extent, it is hypothetical, because it is defined as the change in net irradiance (solar plus long wave) at the tropopause *after allowing the stratosphere to adapt to a change in radiation, while leaving all conditions in the troposphere unchanged*.

The concept of radiative forcing cannot be used for describing the vertical profile of energy balance distortion caused by a forcing agent. However, the vertical variation in forcing may cause certain forcing agents to have a larger effect on climate, compared to other agents for the same amount of radiative forcing (at the tropopause). To take this 'efficacy of radiative forcing' into account, IMAGE 2.5 uses the capacity per unit radiative forcing to change surface temperatures compared to a unit forcing in O_2 (specific value for each agent).

In addition, IMAGE 2.5 uses patterns to distribute the forcing of all forcing agents (including well-mixed gases) over the four land/ocean boxes. This introduces another modification of climate impact for each agent, because land and ocean respond differently. For well-mixed gases, the horizontal pattern of relative forcing is close to unity (Meinshausen *et al.*, 2008).

2.3 Update of radiative forcing agents

With the update to MAGICC 6.0, several forcing agents were added that, so far, had not been accounted for in AOS: NO_3 emissions, Black Carbon, and Organic Carbon are included in image 2.5. In addition, the parameterisation forcing was updated for the following species: direct aerosol effect, indirect aerosol effect, stratospheric ozone depletion, and stratospheric water-vapour forcing by CH_4 abundance. Also the forcing for chlorides, PFCs and HFCs were updated to the IPCC AR4 values (See source-code files 'radiat.const' and 'radiatAR4.const'. Only some forcings changed).

3

Testing the IMAGE-AOS update

The major update of the climate-system component described in the previous chapter requires careful evaluation of the impact on the simulation results of the IMAGE model. Two important issues are discussed in this chapter:

- How do the results from the new model compare to those from the new MAGICC version and the previous IMAGE version?
- What is the impact of variations in new parameters on the IMAGE results, in particular, the CO₂ concentration, which has been calibrated against historical records?

The first section presents a comparison of the new IMAGE model with the MAGICC model and illustrates the impact of two new parameterisations in the models. In the second section is checked whether the CO₂ concentration in the new IMAGE model is sufficiently close to observations from the historical record. In the last section, a comparison is given of the simulation results from the new IMAGE model, in general, with the previous version, for two different scenarios.

3.1 Comparing to MAGICC 6.0 and testing new parameters

Because not all components of the MAGICC model have been implemented in the IMAGE model, we compare the models MAGICC and IMAGE 2.5 only for an ‘equal-forcing’ experiment. In such experiments, both models are fed by equal pathways of radiative forcing for each geographical box, bypassing the components that calculate GHG concentrations and forcings from emission data. Figure 3.1 presents the results from an experiment with historical forcing from 1765 to 2000 (including changes in solar irradiance and volcanic forcing), SRES scenario A1b from 2000 to 2100, and constant forcing

following the year 2100, applied to the time period 2100 to 2300. The parameter setting used in this experiment is provided in Table 3.1.

For this scenario the IMAGE model reproduces MAGICC’s results closely (Figure 3.1). Because it also does for other scenarios and parameter settings (not shown) this means the amendments in the new MAGICC model have been implemented correctly in IMAGE. This also means that it is unlikely that one of the models contains major programming errors, since the programming code was written independently for each model.

Taking the parameter setting in the table above as a starting point, two experiments were performed to illustrate the impact of new parameterisation on IMAGE results (in terms of mean global, and northern hemisphere land temperature change). In the first run, the value of ξ was changed to 0.075 °C·W⁻¹·m². This increased the sensitivity of the climate system to any radiative forcing higher than ΔQ_{2x} (see Section 2.2.1). Figure 3.2 shows that, in this case (‘Qsens’, red/pink lines), the temperature increased more after 2050, compared to the =0 case (black/grey lines).

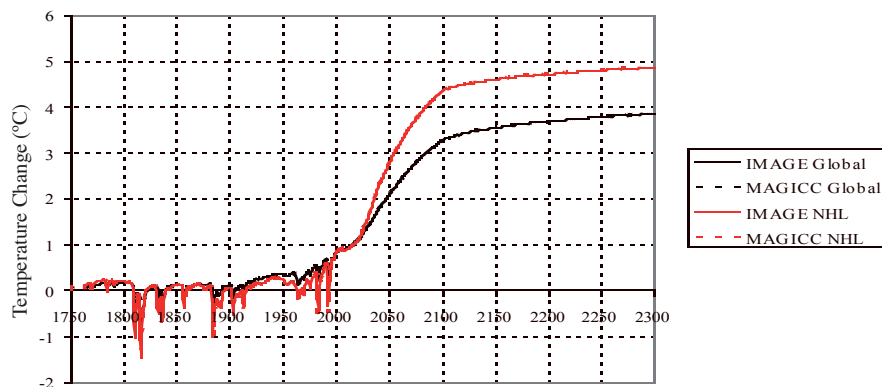
In a second experiment, κ was set to -0.5 cm²·s⁻¹·°C⁻¹. This means that vertical diffusivity decreases as the contrast in temperature change between the top and bottom layers increased, thus reflecting increased stratification of ocean layers and decreased heat diffusion of the warm top layers to the deep ocean. Figure 3.2 shows that, in this case (‘Ksens’, blue lines), the temperature increases faster while the forcing increases (until 2100), but slowed down after concentrations are held fixed (for the period 2100 to 2300). The reason is that, because of increased stratification, the top ocean layer

Parameter settings used in the “equal forcing” experiment

Table 3.1

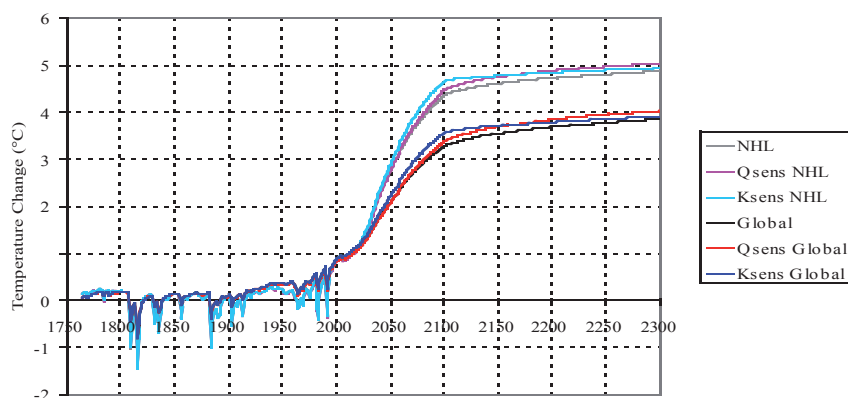
Parameter	Value	Parameter	Value	Parameter	Value
ΔT_{2x}	3.0 °C	$\frac{\partial K_{ztop}}{\partial T}$	0.0 cm ² ·s ⁻¹ ·°C ⁻¹	ΔT^*	8.0 °C
ξ	0.0 °C·W ⁻¹ ·m ²	π	0.2	k_{LO}	0.5 Wm ⁻² ·°C ⁻¹
$K_{z,0}$	1.27 cm ² ·s ⁻¹	w_0	4.0 m·yr ⁻¹	k_{NS}	0.2 Wm ⁻² ·°C ⁻¹
$K_{z,min}$	0.1 cm ² ·s ⁻¹	Constant part w	30%	μ	1.0

Figure 3.1



Results from the MAGICC and IMAGE 2.5 climate models compared for an equal-forcing scenario. Changes are given for mean global (Global) and Northern-Hemisphere-Land (NHL) temperatures, compared to pre-industrial levels.

Figure 3.2



Results from the new IMAGE climate 2.5 model for different parameter settings. Changes are given for mean global (Global) and Northern-Hemisphere-Land (NHL) temperatures, compared to pre-industrial levels.

effectively becomes decoupled from the cooler deep ocean. This means that the top layer responds faster to changes in forcing, but the system needs more time to reach equilibrium with the deep ocean after concentrations, and thus forcing, are stabilised. This slower approach to equilibrium causes the ‘Ksens’ temperature curves to cross the ‘Qsens’ curves after 2150, and the ‘default’ curves to do so sometime after 2300.

Note that, in these experiments, the climate core was effectively decoupled from the rest of the IMAGE model, so interactions and feedbacks play no role. Therefore, the effect of changing these parameters in the full IMAGE model, including feedbacks, may well be stronger or weaker.

3.2 CO₂ concentration

The IMAGE 2.3 model had been calibrated so that the spin-up of the model from 1765 to the present day, reproduced

observed CO₂ concentrations. After implementation of the new MAGICC 6.0 parameterisations and parameter values, one needs to check if re-calibration is required. We have run the new model with parameter settings that allow it to (1) mimic the IMAGE 2.3 response, and (2) emulate the climate response of three state-of-the-art AOGCMs, for which MAGICC parameters were adjusted by Meinshausen *et al.* (2008) (see Section 3.4).

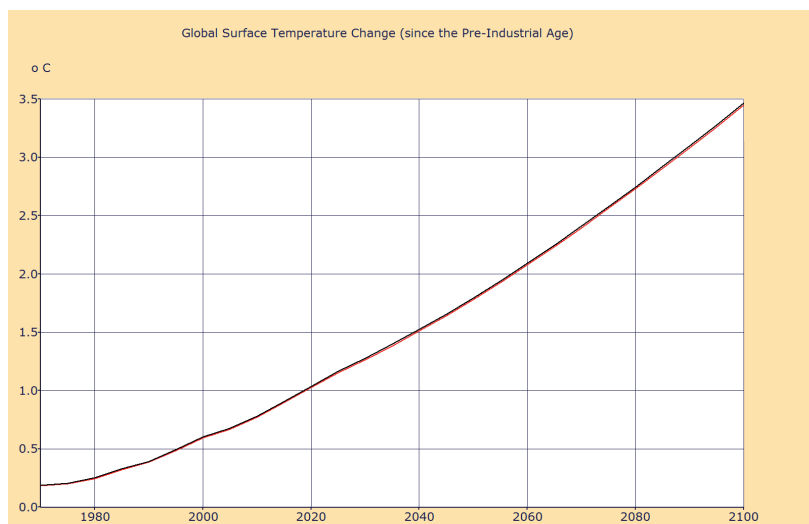
Table 3.2 provides the CO₂ concentration in the year 2000, used for these experiments. The concentrations are sufficiently close to that in IMAGE 2.3, so that no re-calibration was required.

3.3 Comparison with IMAGE 2.3

Including only the changes in the parameterisation of the climate response, we performed experiments for

	IMAGE 2.3	IMAGE 2.5-2.3	IM25-HadCM3	IM25-ECHAM5	IM25-CCSM3	Literature
pCO ₂ 2000 (ppmv)	370.1	370.2	373.0	371.3	370.2	368.90

Figure 3.3



Mean global near-surface air temperatures for SRES A2 scenarios in IMAGE 2.3 (black) and in IMAGE 2.5 (red) with the parameter setting of IMAGE 2.3.

the SRES A2 scenario (high emissions). Provided that the new parameterisation of radiative forcing was not used, IMAGE 2.5 reproduced IMAGE 2.3 results, when parameters were set to the same values as in IMAGE 2.3, and the new parameterisations in IMAGE 2.5 were ‘switched off’ (see mean global temperature change in Figure 3.3). However, small numerical differences exist, because some of the new parameterisations in IMAGE 2.5 required a different programming of equations. Please also note that radiative forcing from BC/OC was excluded in these experiments.

3.4 Scenario projections for various AOGCM emulations

The single most important advantage of the new AOS module in the IMAGE model is its ability to emulate the climate response of AOGCMs. For this purpose, Meinshausen *et al.* (2008) have tuned a set of parameters in the new MAGICC model. Indeed, the main purpose of the MAGICC update and the new parameterisations in the model – which meanwhile have been included in the new IMAGE version – was to better reproduce the behaviour in time of AOGCMs. In previous IMAGE versions, the geographical patterns of climate change were provided by the output of a range of AOGCMs (as it is in the new version), but the pathway in time of these changes was given by the default dynamics of the previous IMAGE-AOS. In IMAGE 2.5, the patterns can be coupled to the time dependency of the AOGCM in question, for a more consistent projection of long-term mean climate change and its impacts.

To illustrate the new ‘feature’ of mimicking the time dependency of AOGCMs, we adjusted the parameters in

IMAGE to emulate three of the most advanced AOGCMs: HadCM3, ECHAM5 and CCSM3, from, respectively, Hadley Centre (United Kingdom), Max Planck Institute (Germany) and National Centre of Atmospheric Research (United States). The parameter settings are given in the table below, including the parameter setting that permits IMAGE 2.5 to mimic the behaviour of IMAGE 2.3. The parameter settings that allow IMAGE 2.5 to emulate the AOGCMs are simply referred to as ‘the models’. Thus, the ‘HadCM3’ experiment obviously does not refer to an experiment using the HadCM3 model, but rather the IMAGE 2.5 model with a parameter setting emulating HadCM3 behaviour.

For each model (parameter setting), we have performed experiments for the SRES A2 scenario (high emissions) and the SRES A1B-450 scenario, stabilising CO₂ concentrations below 450 ppmv from a SRES A1B baseline scenario. These scenarios provide an estimate of two extremes in the range of plausible GHG-concentration pathways. They serve to illustrate the variation in climate projections resulting from the various parameter settings.

Figure 3.4 shows that, for all models, the mean global temperature change stays below 2 °C in the A1B-450 scenario, while it exceeds 4 °C in the A2 scenario. Note that the mean global temperature change in these realisations of the SRES A2 scenario did not equal the results from the AOGCM experiments for two major reasons: 1) the SRES marker scenarios used for driving the AOGCMs in, for example, the Fourth Assessment Report of IPCC, generally have lower emissions and CO₂-equivalent concentrations than the IMAGE versions of these scenarios, and (2) the experiments for this

The parameter settings to emulate the behaviour of different AOGCMs (three examples), and to reproduce the behaviour of IMAGE 2.3. These parameters are implemented in the AOGCM-specific aos_const files, which can be chosen from the file 'const_filenames.dat'

Table 3.3

Parameter	IMAGE 2.3	HadCM3	ECHAM5	CCSM3
$\Delta T_{2\sigma}$ ($^{\circ}\text{C}$)	2.50	3.21	3.23	2.14
($\text{W}\cdot\text{m}^{-2}$)	5.325	5.500	5.790	5.699
ξ ($^{\circ}\text{C}\cdot\text{W}^{-1}\cdot\text{m}^2$)	0.000	0.000	0.075	0.064
RLO	1.20	1.59	1.52	1.37
$f_{\text{NH}} f_{\text{SH}}$	0.42 0.21	0.47 0.23	0.44 0.22	0.49 0.25
K_{so} ($\text{cm}^2\cdot\text{s}^{-1}$)	2.30	1.59	0.61	1.27
$\frac{\partial K_{\text{stop}}}{\partial T}$ ($\text{cm}^2\cdot\text{s}^{-1}\cdot^{\circ}\text{C}^{-1}$)	0.00	0.00	-0.06	-0.21
Constant part w	70%	30%	30%	30%
k_{LO} ($\text{W}\cdot\text{m}^{-2}\cdot^{\circ}\text{C}^{-1}$)	1.00	4.00	4.00	4.00
k_{NS} ($\text{W}\cdot\text{m}^{-2}\cdot^{\circ}\text{C}^{-1}$)	1.00	1.12	2.44	0.40
μ	1.00	1.39	1.25	1.22

Global Surface Temperature Change (since the Pre-Industrial Age)

Figure 3.4



Mean global near-surface air temperature change in the SRES A2 (top lines) and SRES A1B-450 (lower lines) scenarios, in IMAGE 2.5, with various parameter settings emulating the behaviour of HadCM3 (black), CCSM3 (red) and ECHAM5 (green).

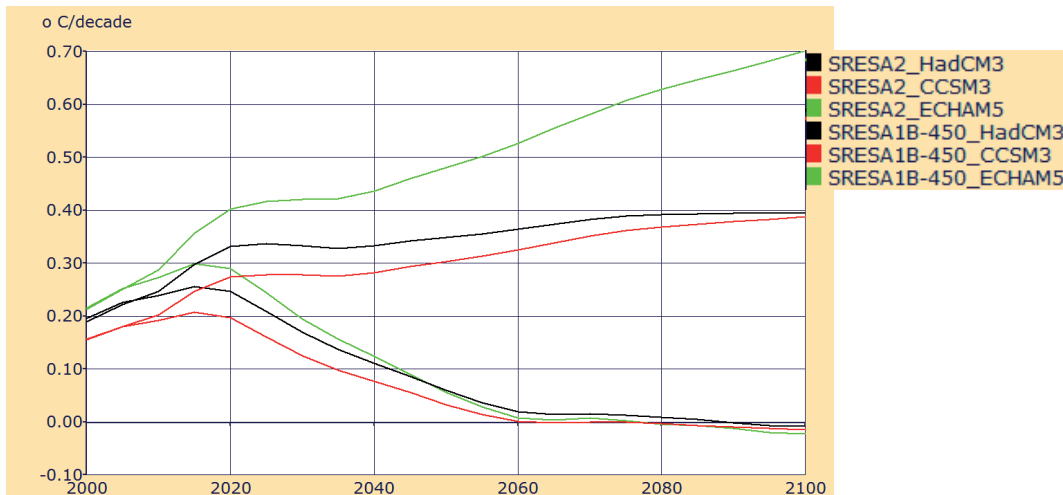
paper were produced using a larger number of greenhouse gases and direct or indirect aerosol effects than were used in the AOGCM experiments.

As can be concluded from Figure 3.4 and, especially, Figure 3.5, the ECHAM5 model responds much more rapidly and more extreme than the other models. This is due to a combination of parameter settings: (1) the climate sensitivity increases for high forcing ($\xi > 0$), hence, the extreme response in the A2 scenario, while for the A1B-450 scenario, the response stays close to HadCM3; (2) the initial ocean diffusivity is much lower, thus decoupling the ocean mixed layer from the deep ocean, which increased the speed of response (Figure 3.5); (3) the initial climate sensitivity ($\Delta T_{2\sigma}$) is highest for ECHAM5, while (4) the radiative response to CO_2 (α_{CO_2}) is also highest. In general, the response of CCSM3 is low, because of the low climate sensitivity and radiative response

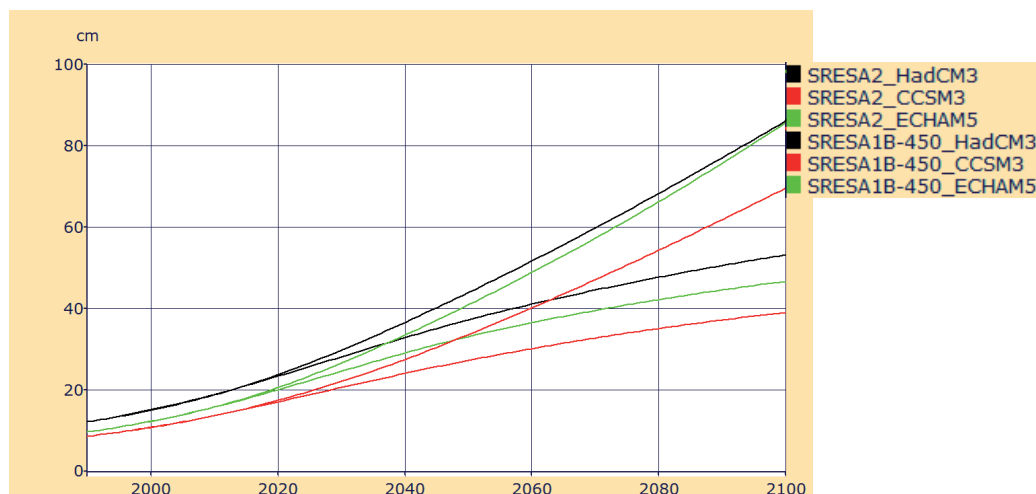
to CO_2 , but caught up for higher forcings, because its sensitivity increased ($\xi > 0$), together with its responsiveness

(decreasing ocean diffusivity, $\frac{\partial K_{\text{stop}}}{\partial T} < 0$).

The low vertical diffusion in ECHAM5 meant that heat penetrated the deep ocean slowly, resulting in a modest sea level rise from ocean-layer expansion (Figure 3.6). However, because of the stronger warming in ECHAM5 in the A2 scenario, sea level rise would catch up with HadCM3 by the late 21st century.



Decadal rate of mean global near-surface air temperature change in the SRES A2 (top lines) and SRES A1B-450 (lower lines) scenarios, in IMAGE 2.5, with various parameter settings emulating the behaviour of HadCM3 (black), CCSM3 (red) and ECHAM5 (green).

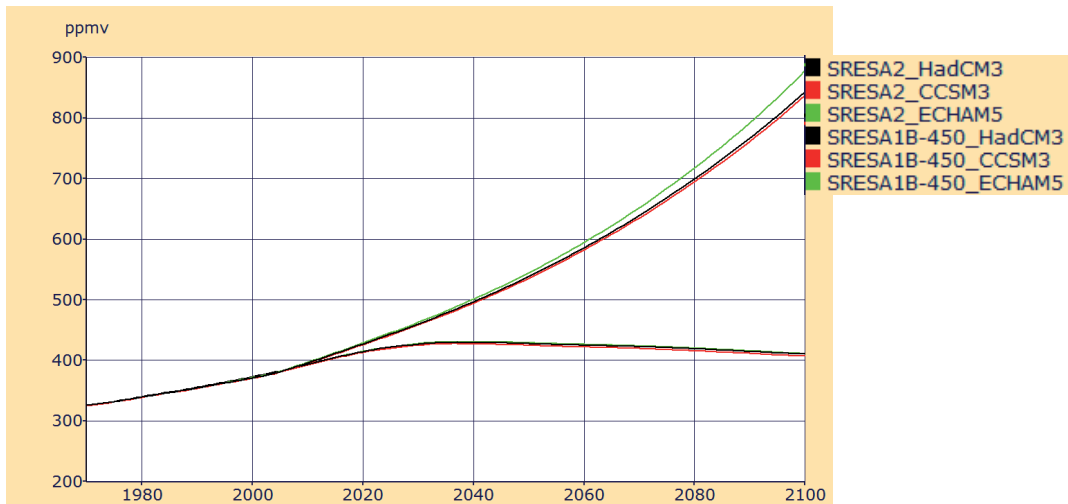


Sea level rise in the SRES A2 (top lines) and SRES A1B-450 (lower lines) scenarios, in IMAGE 2.5, with various parameter settings emulating the behaviour of HadCM3 (black), CCSM3 (red) and ECHAM5 (green).

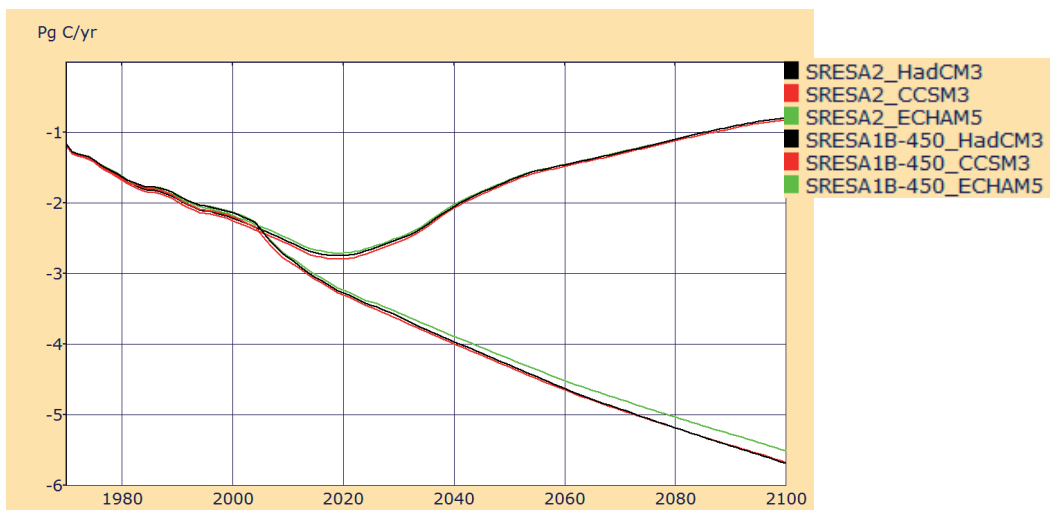
At the end of the A2 simulations, ECHAM5 also appeared an extreme case in terms of CO₂ concentration (Figure 3.7). This is partly due to the lower CO₂ uptake by the oceans (Figure 3.8), but more importantly, also due to the lower net uptake by terrestrial vegetation (Figure 3.9). While net primary productivity (not shown) for HadCM3 and ECHAM5 stays virtually equal, soil respiration in ECHAM5 increases relative to HadCM3 (Figure 3.10).

in Figure 3.11, the response of ECHAM5 posed a much higher threat to natural vegetation than that of HadCM3, for the same SRES A2 scenario.

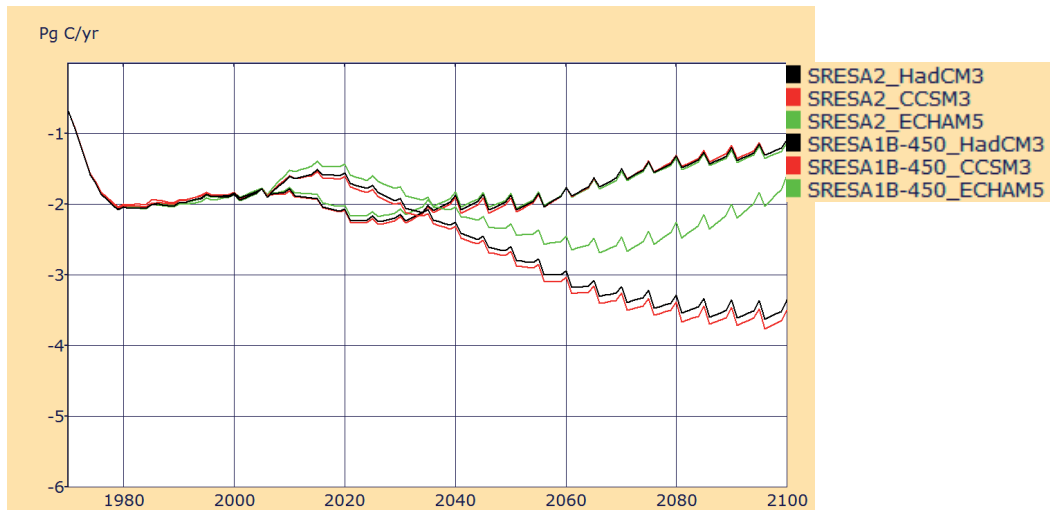
A final impact worth noting here is that resulting from the difference in rate of change. Because this was much higher in ECHAM5, natural vegetation would have much less time to adjust, for example, by migration. Indeed, as can be seen



CO₂ concentration in the SRES A2 (top lines) and SRES A1B-450 (lower lines) scenarios, in IMAGE 2.5, with various parameter settings emulating the behaviour of HadCM₃ (black), CCSM₃ (red) and ECHAM₅ (green).



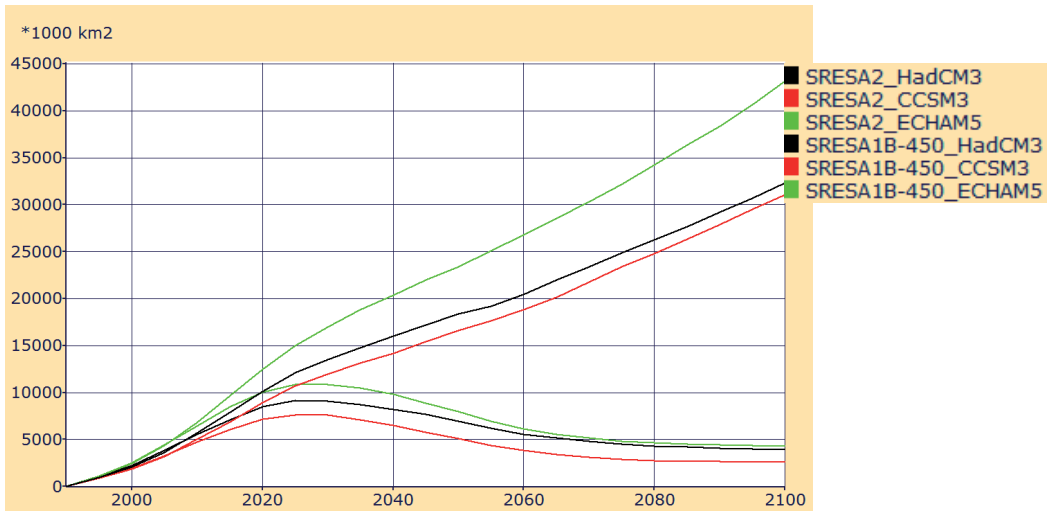
Ocean carbon uptake in the SRES A2 (lower lines) and SRES A1B-450 (top lines) scenarios, in IMAGE 2.5, with various parameter settings emulating the behaviour of HadCM₃, ECHAM₅ and CCSM₃.



Terrestrial vegetation carbon uptake in the SRES A2 (lower lines) and SRES A1B-450 (top lines) scenarios, in IMAGE 2.5, with various parameter settings emulating the behaviour of HadCM3



Figure 3.10. Soil respiration flux for SRES A2 (top lines) and SRES A1B-450 (lower lines) scenarios, in IMAGE 2.5, with various parameter settings emulating the behaviour of HadCM3 (black), CCSM3 (red) and ECHAM5 (green).



Threat to natural vegetation in IMAGE 2.5: the area (total for all terrestrial vegetation classes) of vegetation that is confronted with a rate of climate change than is higher than its adaptive capacity. Shown are the results of three parameter settings: HadCM₃ (black), CCSM₃ (red) and ECHAM₅ (green) for two scenarios: SRES-A₂ (top lines) and SRESA1B-450 stabilisation (lower lines).

Conclusions

4

Implementing the changes to the MAGICC model, as given by Meinshausen *et al.* (2008), in the IMAGE model, allows the model to emulate the time-dependent climate response of AOGCMs to radiative forcing. The geographical pattern scaling in the IMAGE model, that scales climate change patterns from AOGCM experiments, can now be combined with the 'correct' dynamic response in time. This dynamic response (without the consistent link to climate change patterns) has been illustrated in this report for three AOGCMs, showing that the effect on climate change impacts can be large. This extends the range of uncertainty that can be covered by the IMAGE model in its projections of future climate change and the impacts thereof. In addition, its projections can be made much more physically consistent when the parameter setting that allows the IMAGE model to emulate the dynamic response of a certain AOGCM, is also combined with geographical pattern scaling using output of the same AOGCM.

References

- de Haan BJ, Jonas M, Klepper O, Krabek J, Krol MS, Olendrzynki K (1994) An atmosphere-ocean model for integrated assessment of global change. *Water, Air and Soil Pollution* 76:283-318
- Eickhout B, den Elzen MGJ, Kreileman GJJ (2004) The Atmosphere-Ocean System of IMAGE 2.2: A global model approach for atmospheric concentrations, and climate and sea level projections, National Institute for Public Health and the Environment (RIVM), Bilthoven
- Forster P, Ramaswamy V, Artaxo P, Bernsten T, Betts R, Fahey DW, Haywood J, Lean J, Lowe DC, Myhre N, Nganga J, Prinn R, Raga G, Schulz M, Van Dorland R (2007) Changes in atmospheric constituents and in radiative forcing. In: Solomon S, Qin D, Manning M, Marquis M, Averyt K, Tignor MMB, Miller Jr. HL, Chen Z (eds) *Climate Change 2007: The Physical Science Basis. Contribution of Working Group I to the Fourth Assessment Report of the Intergovernmental Panel on Climate Change*. Cambridge University Press, New York, USA, p 129-234
- Hansen J, Sato M, Ruedy R, Nazarenko L, Lacis A, Schmidt GA, Russell G, Aleinov I, Bauer M, Bauer S, Bell N, Cairns B, Canuto V, Chandler M, Cheng Y, Del Genio A, Faluvegi G, Fleming E, Friend A, Hall T, Jackman C, Kelley M, Kiang N, Koch D, Lean J, Lerner J, Lo K, Menon S, Miller R, Minnis P, Novakov T, Oinas V, Perlwitz J, Perlwitz J, Rind D, Romanou A, Shindell D, Stone P, Sun S, Tausnev N, Thresher D, Wielicki B, Wong T, Yao M, Zhang S (2005) Efficacy of climate forcings. *Journal of Geophysical Research* 110:D18104
- Harvey D, Gregory J, Hoffert M, Jain A, Lal M, Leemans R, Raper S, Wigley T, de Wolde J (1997) An introduction to simple climate models used in the IPCC Second Assessment Report, Intergovernmental Panel on Climate Change (IPCC), Geneva
- Houghton JT, Meira Filho LG, Callander BA, Harris N, Kattenberg A, Maskell K (eds) (1996) *Climate Change 1995: The science of climate change. Contribution of Working Group I to the Second Assessment Report of the Intergovernmental Panel on Climate Change, Vol. Cambridge University Press, Cambridge, United Kingdom, New York, NY, U.S.A. and Melbourne, Australia*
- Hulme M, Wigley T, Barrow E, Raper S, Centella A, Smith S, Chipanski A (2000) Using a climate scenario generator for vulnerability and adaptation assessments: MAGICC and SCENGEN version 2.4 workbook, Norwich, UK
- IMAGE-team (2001) The IMAGE 2.2 implementation of the SRES scenarios. A comprehensive analysis of emissions, climate change and impacts in the 21st century. Main disc. National Institute for Public Health and the Environment (RIVM), Bilthoven, the Netherlands.
- IPCC (2001) *Climate Change 2001: The scientific basis, Vol. Cambridge University Press, Cambridge*
- Joos F, Bruno M, Fink R, Siegenthaler U, Stocker TF, Le Quéré C, Sarmiento JL (1996) An efficient and accurate representation of complex oceanic and biospheric models of anthropogenic carbon uptake. *Tellus* 48B:397-417
- Krol MS, van der Woerd H (1994) Atmospheric composition calculation for evaluation of climate scenarios. *Water, Air and Soil Pollution* 76:259-281
- Meehl GA, Stocker TF, Collins WD, Friedlingstein P, Gaye AT, Gregory JM, Kitoh A, Knutti R, Murphy JM, Noda A, Raper SCB, Watterson IG, Weaver AJ, Zhao Z-C (2007) Global Climate Projections. In: Solomon S, Qin D, Manning M, Marquis M, Averyt K, Tignor MMB, Miller Jr. HL, Chen Z (eds) *Climate Change 2007: The Physical Science Basis. Contribution of Working Group I to the Fourth Assessment Report of the Intergovernmental Panel on Climate Change*. Cambridge University Press, New York, USA, p 747-845
- Meinshausen M, Raper S, Wigley T (2008) Emulating IPCC AR4 atmosphere-ocean and carbon cycle models for projecting global-mean, hemispheric and land/ocean temperatures. *Atmospheric Chemistry and Physics Discussions* 8 (2), pp. 6153-6272
- Raper SCB, Cubasch U (1996) Emulation of the results from a coupled general circulation model using a simple climate model. *geophysical research letters* 23:1107-1110
- Raper SCB, Gregory JM, Osborn TJ (2001) Use of an upwelling-diffusion energy balance climate model to simulate and diagnose A/OGCM results. *Climate Dynamics* 17:601-613
- Raper SCB, Wigley TML, Warrick RA (1996) Global sea-level rise: Past and future. In: Milliman JD, Haq BU (eds) *Sea-level rise and coastal subsidence*. Kluwer academic publishers, p 11-45
- Schlesinger ME, Malyshev S, Rozanov EV, al. e (2000) Geographical distributions of temperature change for scenarios of greenhouse gas and sulfur dioxide emissions. *Technological Forecasting and Social Change* 65:167-193
- Wigley TML, Raper SCB (1987) Thermal expansion of sea water associated with global warming. *nature* 330:127-131
- Wigley TML, Raper SCB (1992) Implications for climate and sea level of revised IPCC emissions scenarios. *Nature* 357:293-300
- Wigley TML, Raper SCB (1993) Future changes in global mean temperature and sea level. In: Warrick RA, Barrow EM, Wigley TML (eds) *Climate and sea level change: observations, projections and implications*. Cambridge University Press, Cambridge
- Wigley TML, Raper SCB (1995) An heuristic model for sea level rise due to the melting of small glaciers. *Geophysical Research Letters* 22:2749-2752
- Wigley TML, Schlesinger ME (1985) Analytical solution for the effect of increasing CO₂ on global mean temperature. *nature* 315:649-652

Colophon

Responsibility

Netherlands Environmental Assessment Agency (PBL)

Authors

Michiel Schaeffer, Elke Stehfest

Lay out

Studio RIVM

Contact

Elke.Stehfest@pbl.nl

IMAGE-info@pbl.nl

We are very grateful to Malte Meinshausen who developed MAGICC 6.0 and the parameter sets to emulate GCM results, provided the MAGICC source code to us for reference and supported the implementation in IMAGE.

From PBL side, Elke Stehfest supported and supervised the work, and did the final editing of the report.

Descriptions of the unchanged parts of the IMAGE climate system were adopted from Eickhout et al. 2004.

The climate subsystem in IMAGE updated to MAGICC 6.0

The simple climate model MAGICC is part of the Atmosphere-Ocean System (AOS) within the IMAGE model (“Integrated Model to Assess the Global Environment”) of PBL. The MAGICC model was used extensively in the Third and Fourth Assessment Reports of IPCC (Intergovernmental Panel on Climate Change) for running a range of greenhouse gas concentration scenarios. Since publication of these reports, the MAGICC model has been updated to improve its emulation of results from Atmosphere-Ocean General Circulation Models (AOGCMs). The series of improvements to the MAGICC model have been implemented in IMAGE-AOS, to bring IMAGE 2.5 up-to-date with the most recent developments in climate modelling. This report presents details about the improvements and the re-calibration of the model, it shows the model results and discusses the similarities and differences with the previous IMAGE versions and the new MAGICC 6.0 version.

The single most important advantage of the new IMAGE model is that, in combination with MAGICC 6.0, the model can reproduce the time-dependent response of AOGCMs for various scenarios, by adjusting the values of a limited number of parameters. This makes the IMAGE model better suited to provide plausible projections of future climate-change feedbacks and impacts.